Supporting Information for

Incubated protein reduction and digestion on an EWOD digital microfluidic chip for MALDI-MS

Wyatt C. Nelson,*[a] Ivory Peng,[b] Geun-An Lee,[c] Joseph A. Loo,[b,d] Robin L. Garrell,[b] and Chang-Jin "CJ" Kim.[a]

[a]Mechanical and Aerospace Engineering Department, University of California, Los Angeles (UCLA), 420 Westwood Plaza, Engineering IV Room 37-129, Los Angeles, CA 90095, USA.
[b]Department of Chemistry and Biochemistry, Univeristy of California, Los Angeles (UCLA), Los Angeles, CA 90095-1569, USA.
[c]Korea Institute of Industrial Technology, Incheon, Korea.
[d]Department of Biological Chemistry, David Geffen School of Medicine, University of California, Los Angeles (UCLA), Los Angeles, CA 90095, USA.

wyattnelson@ucla.edu

Contents:

S-1. Operating principles for droplet actuation and heating using multifunctional electrodes

S-2. EWOD chip fabrication process flow

S-3. Control system diagram

S-4. Heater time histories and calibration data

S-5. Description of experimental and numerical thermal modeling

S-1. Operating Principles of Multifunctional Electrodes

Multifunctional electrodes are designed to employ different transduction mechanisms for droplet driving and temperature control. The force driving droplet movement is electrostatic; the Joule heating and thermistic temperature sensing are resistive. Figure S-1 shows top-view and cross-sectional schematics showing the operating principles for movement and heating, which are activated and deactivated by electrical switching. To move the sample onto the heater by EWOD (Figure S-1a), a voltage is applied across the top electrode and bottom electrodes. To heat the sample by resistive heating, on the other hand, the heater electrode is disconnected from the top electrode and closed with its own applied potential (Figure S-1b).

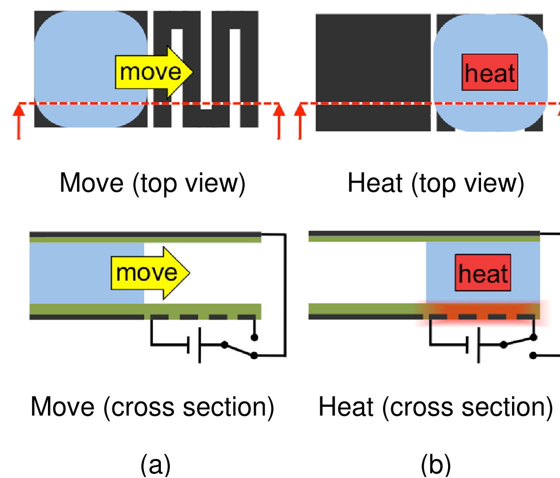

Figure S-1: Operating principles for multifunctional electrodes: the droplet moves when a potential is applied to the heater, and the droplet is heated when current is passed through the heater.

S-2. Fabrication Process Flow

Figure S-2 illustrates the process flow, including a top view of ITO and gold layers. The substrate is a 700 μm thick glass wafer coated with 140 nm ITO by the manufacturer (TechGophers Co.). Photoresist (AZ 5214) is spin-coated on 200/10 nm evaporated gold/chromium and patterned by ultraviolet (UV) exposure and development, defining the ITO electrode layout. The gold layer and chromium adhesion layer are then wet etched, followed by ITO wet etching in 5 wt % oxalic acid. Gold and chromium are wet etched again, masked by another photoresist layer, to form heater leads, and 1 μm silicon nitride is deposited by plasma-enhanced chemical vapor deposition (PECVD). A hydrophobic polymer, 6 wt % Cytop®, is spin-coated at 2000 rpm for 30 s, giving a thickness of 200 nm. In some cases, the Cytop® was etched by oxygen plasma to form hydrophilic rings on heaters. Device top plates were fabricated by spin-coating 200 nm Cytop® onto a blank ITO-coated glass wafer. Cytop® fluoropolymer and solvent solutions were purchased from Asahi Glass Co., Ltd. (Japan). The University of California, Los Angeles (UCLA) Nanoelectronics Facility (NRF), provided chemicals for wet and dry microfabrication.

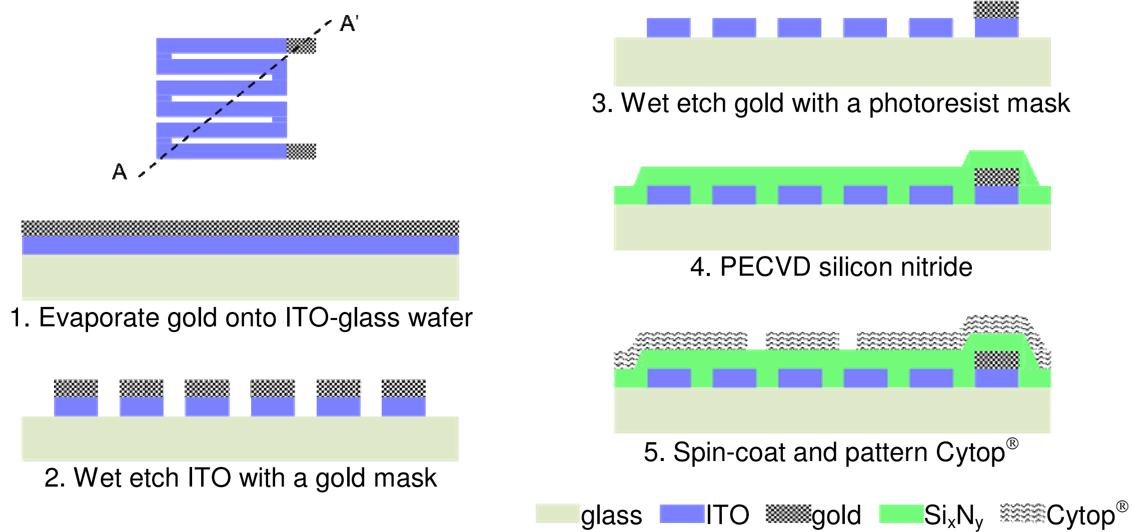

Figure S-2: (a) Top view of a multifunctional electrode (heater/sensor/EWOD pad). (b) Process flow: First, 200 nm gold (upon a 10 nm chromium adhesion layer) is evaporated onto a commercially coated ITO-glass wafer. Second, gold, chromium, and ITO are wet etched. Third, gold is wet etched to form heater leads. Fourth, 1 μm PECVD nitride is coated, and finally 200 nm Cytop is spin-coated and plasma etched.

S-3. System Diagram

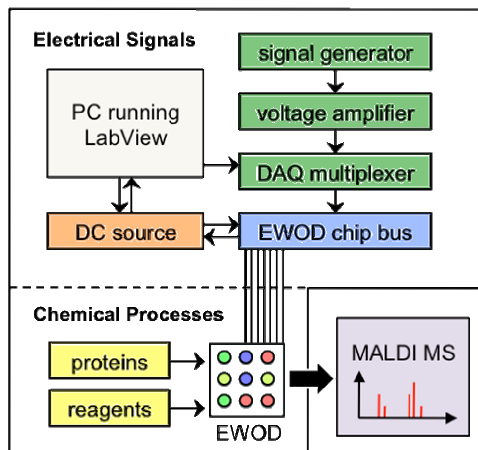

Figure S-3: A system diagram in which electrical signals controlled by a computer running LabView are translated into chemical processes on the EWOD chip. Actuation voltage from the signal generator and amplifier is routed through the DAQ multiplexer. Heating current is supplied to the chip and measured by a DC power source under PID control.

S-4. Heater Time Histories

The thermistic relationship between temperature and electrical resistance can be linear over certain temperature ranges and is quantified by the temperature coefficient of resistance (TCR). From experimental data and Equation S-4.1, we calculated a TCR of about 0.0008 K^{-1} for the thin-film ITO heaters.

$$TCR = \left(\Delta R / R_0\right) / \Delta T \tag{S-4.1}$$

The inset of Figure S-4 shows our calibration curve, obtained by measuring heater resistances with a thermocouple attached to the chip. The chip was immersed in a transformer oil bath held at a range of stable temperatures from room temperature to 150 °C. There is a linear relationship, and our PID control used the TCR value as the proportionality relating measured resistance values to heater temperature.

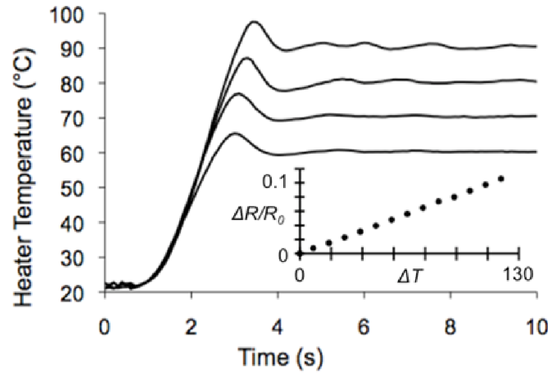

Figure S-4. Heater temperature time history for 1 μL water droplet (initial radius ≈ 1.5 mm, thickness ≈ 100 μm) on a 3 mm x 3 mm heater. The inset shows ITO temperature coefficient of resistance, i.e., $\Delta R/R_0$ vs. ΔT ($0 \leq \Delta T \leq 130$ °C) calibration plot.

S-5. Modeling of Thermal Characteristics

Three-dimensional numerical simulations were performed to generate a temperature map of the chip during heating of a single water droplet at constant temperature for one minute. Figure S-5a is a simplified schematic of our finite element model, with a reference coordination system placed at the center bottom of the droplet. The three dimensional transient heat diffusion equation (modeling solid body heat conduction with convective boundary conditions and temperature-dependent conductivities) was solved over a mesh that accounted for every layer of the device: ITO, silicon nitride, and Cytop on the bottom glass plate, and ITO and Cytop on the top glass plate. Since the purpose of this numerical analysis is to check chip temperatures away from a heated droplet, and not variations within the heater or droplet, the heater is treated as a uniform hot spot and thus given a constant temperature boundary condition. For modeling the heater itself, a heat flux condition would have been needed.

A test device was fabricated in order to compare measured temperatures with simulation results. The experimental values, tracked using ITO thermistors located at various distances from a heater, are plotted in Figure 5-Sb along with simulation results corresponding to heating time = 60 s and y = 0, z = 0, and $0 \leq x \leq 10$ heater lengths. There is good agreement between simulation and experiment, considering the complexity of the system.

Droplets surrounded by air evaporate during heating experiments. Our simulation uses an adjusted heat transfer coefficient h_{evap} for the liquid/gas interface in order to account for the volume loss due to evaporation. This coefficient was estimated from experimentally measured values of droplet radius on a heater at 70 °C for 60 s. We assume the energy carried away from the droplet by water vapor, (volume change) × (enthalpy of vaporization), is the total energy transferred across the interface, h_{evap}× (area) × (temperature change) × (time). Equating these quantities yields the following for a cylindrical (disk-like) droplet:

$$h_{\text{evap, 70 °C, 60 s}} = \frac{\Delta_v H \cdot \rho \left(R^2_{\text{t = 0 s}} - R^2_{\text{t = 60 s}} \right)}{2 \cdot \Delta T \cdot \Delta t \cdot R_{ave}} \approx 200 \text{ W/m}^2\text{K} \qquad \text{(S-5.1)}$$

Equation 3 is a function of the enthalpy of vaporization, $\Delta_v H$ (2333 kJ/kg for water at 70 °C), density ρ ($\rho_{\text{water, 70 °C}} \approx 980$ kg/m^3), droplet radii R at times 0 s and 60 s (1.5 mm and 1.25 mm), average droplet radius R_{ave} (1.38 mm), temperature drop from liquid to ambient ΔT ($\approx$ 48 K), and heating time Δt (60 s),[29] An overall heat transfer coefficient $h_{overall}$ of 20 W/m^{2}K was applied to all glass-air boundaries. This coefficient is an approximation made via $h_{overall}$ = [(DC supply current)^2 × heater resistance] ⁄ [(chip surface) × (temperature change)] ≈ 0.6 W / (0.0006 m^2 x 48 K) ≈ 20 W/m^{2}K. When verified by experimental data (Figure 5b), our simple model, which does not deal with factors including ambient airflow, phase changes within the plate gap, and conduction through the chip bus, provides a reasonable temperature profile and satisfies our goal of mapping heat flow through the chip in its current configuration. With this numerical

method, we form a starting point from which to optimize the design for applications that require extremely low power and high thermal isolation. On the reported device, according to Figure S-5(b), the substrate is predicted to be at room temperature six heater lengths away from a heated droplet. These results represent baseline performance of a chip not optimized for thermal management.

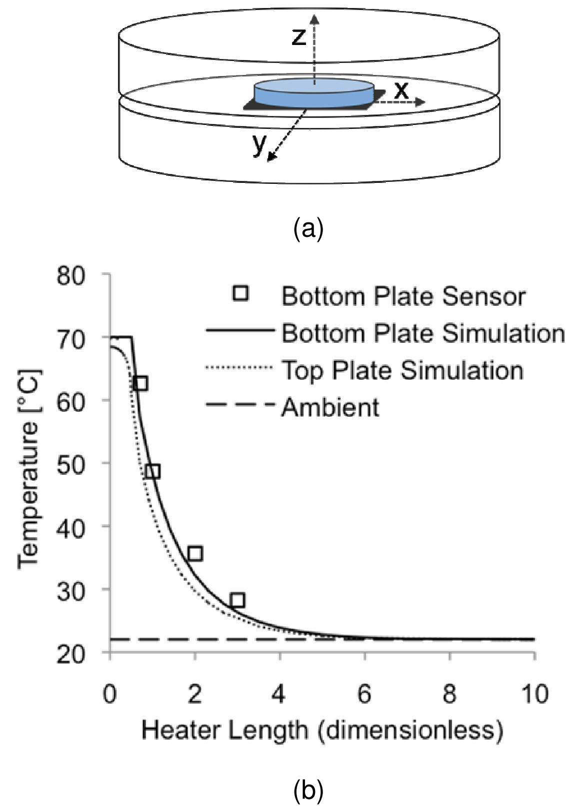

Figure S-5. Three-dimensional heat transfer simulation. (a) Simplified schematic of simulated model (not to scale): A droplet, sandwiched between cylindrical glass plates, sits on a thin-film heater on the lower plate. The entire system is immersed in ambient air. The mesh geometry and parameters of our simulation account for all devices layers. (b) Experimental and simulation results for heating time = 60 s and $y = 0$, $z = 0$, and $0 \leq x \leq$ 10 heater lengths.